Estimation and Model Validation of Surface Solar Radiation and Cloud Radiative Forcing Using TOGA COARE Measurements

MING-DAH CHOU

Laboratory for Atmospheres, NASA/Goddard Space Flight Center, Greenbelt, Maryland,

WENZHONG ZHAO

Applied Research Corporation, Landover, Maryland

(Manuscript received 16 February 1996, in final form 13 July 1996)

ABSTRACT

The Tropical Ocean and Global Atmosphere Coupled Ocean–Atmosphere Response Experiment (TOGA COARE) radiation measurements in the western Pacific warm pool are used to estimate surface solar radiation budgets and to validate radiation model calculations. Clear-sky fluxes are identified from the measurements of direct and diffuse fluxes at the ARM (Atmospheric Radiation Measurements) site of Kavieng by simultaneously imposing conditions that 1) the direct downward solar flux is a maximum, 2) the diffuse downward solar flux is a minimum, and 3) the total flux varies smoothly with time. Averaged over the four TOGA COARE months, the clear-sky downward solar flux at Kavieng is 308 W m^{-2}, with a range of 302–317 W m^{-2}. The estimated clear-sky solar flux, together with the temperature and humidity radiosondings, are then used to validate radiation model calculations. Using an inferred aerosol optical thickness of 0.12, results show that clear-sky surface solar fluxes can be reliably computed from a radiation model. The effect of clouds on surface solar radiation is found to be large. Averaged over the four TOGA COARE months and the seven radiation stations, the surface cloud radiative forcing is 99 W m^{-2} with a range of 79–112 W m^{-2}. This result of the mean cloud radiative forcing is in agreement with other current studies.

1. Introduction

Clouds have a large effect on the surface solar (shortwave, or SW) heating. In a study of the radiation budgets in the western Pacific warm pool region using satellite observations and model calculations, Chou (1994) found that solar heating of the ocean varied by ≈40 W m^{-2} between an El Niño year and a non-El Niño year, primarily due to the shift of cloudiness between the western equatorial Pacific and the central equatorial Pacific. This large change in solar heating is equivalent to a change of ≈7°C in temperature, if only the radiation balance is considered. The importance of clouds on the surface SW flux is further enhanced by the issue of the effect of clouds on atmospheric heating. Even with a number of currently rejuvenated studies (Arking et al. 1996; Cess et al. 1995; Chou et al. 1995; Hayasaka et al. 1995; Imre 1996; Li and Moreau 1996; Ramanathan et al. 1995; Pilewskie and Valero 1995), uncertainties still remain as to whether clouds enhance or reduce the absorption of SW radiation in the atmosphere. Since the cloud-enhanced (or reduced) SW heating is relative to the heating without clouds, it is important to accurately estimate clear-sky SW heating. Direct validations of the surface SW flux calculations are difficult due to uncertainties in the measurements of SW flux and the lack of concomitant measurements of clouds and atmospheric water vapor, ozone, and aerosol concentrations. Previous studies of the clear-sky SW radiation by comparing radiometer flux measurements with model calculations yielded mixed results (e.g., Charlock and Alberta 1996; Shi 1994). Although some laboratory measurements of the absorption by water vapor are available, those measurements were conducted under conditions that were different from atmospheric conditions.

The Tropical Ocean and Global Atmosphere Coupled Ocean–Atmosphere Research Experiment (TOGA COARE) conducted during the Intensive Observation Period (IOP), November 1992–February 1993, provided surface measurements of SW flux and radiosonde measurements of temperature and humidity at a number of stations in the western tropical Pacific warm pool. These measurements were used in this study to estimate the surface clear-sky SW flux and to validate radiation model calculations. We also investigate the effect of clouds on the SW heating of the ocean and compare the results with other studies.

Corresponding author address: Dr. Ming-Dah Chou, Code 913, NASA/Goddard Space Flight Center, Greenbelt, MD 20771.
E-mail: chou@climate.gsfc.nasa.gov

TABLE 1. Locations of the seven TOGA COARE radiation stations.

	Longitude	Latitude
IMET	156.00°E	1.76°S
Kapingamarangi	154.80°E	1.07°N
Kavieng	150.80°E	2.58°S
Kexue	156.00°E	4.00°S
Manus	147.43°E	2.06°S
Nauru	166.93°E	0.55°S
Shiyan	158.00°E	2.25°S

2. Data source

During the TOGA COARE IOP, from 1 November 1992 to 28 February 1993, Integrated Sounding System (Parsons et al. 1994) was installed at two island stations (Kavieng, Kapingmarangi) and two ships (Kexue#1, Shiyan#3) in the intensive flux area (IFA) and two island stations (Manus, Nauru) in the outer sounding array (OSA). Latitudes and longitudes of these stations are given in Table 1. The ISS includes a balloon-borne Omega-based NAVID sounding system. Four sondes at 6-h intervals were launched each day to measure atmospheric temperature and humidity profiles. Surface radiation measurements were conducted at these ISS stations, as well as a buoy (IMET) station near the center of IFA. An upward-looking Eppley PSP pyranometer was used to measure SW flux from 0.3 to 3.0 μm at all stations. The factory estimated accuracy of the pyranometer is $\pm 2.3\%$, or ≈ 10–15 W m^{-2}. At the Kavieng station, additional radiation measurements were made as part of the Atmospheric Radiation Measurement (ARM) program, Pilot Radiation Observation Experiment (PROBE), which include the diffuse flux measurement utilizing an Eppley PSP pyranometer fitted with a shading band to block the direct SW radiation (Long 1996). The direct SW flux is obtained by subtracting the diffuse flux from the total flux. High resolution 1-min data are available from all stations, except the IMET buoy station, which has a 7.5-min resolution.

3. Estimation of clear-sky SW flux

In the warm pool region during TOGA COARE IOP, convection was strong and cloud cover was large. Even in relatively calm periods between the two westerly wind-burst episodes (27 December 1992–6 January 1993; 23 January 1993–3 February 1993), low-level clouds appeared to be ubiquitous. Identification of clear-sky fluxes is difficult due to complex cloud situations. When clouds are present but do not block the direct sunlight, the surface SW radiation will exceed the clear-sky radiation due to the extra radiation scattered by ''lingering'' clouds. Thus, the maximum surface SW radiation, for a given local time, often corresponds to the radiation in a partly cloudy sky (Arking et al. 1996). Our analysis of the TOGA COARE surface radiation data shows that there are only a limited number of cases where the surface radiation varies smoothly over a period longer than a few hours, indicating a strong interference of surface radiation by clouds. The surface radiation varies with humidity and aerosols, which further complicate the estimation of clear-sky SW radiation.

In a study of the cloud effect on the surface SW radiation during TOGA COARE, Waliser et al. (1996) used both the total downward SW flux measured at the IMET buoy and the visible albedo, $\alpha_{\rm vis}$, measured by the Geostationary Meteorological Satellite (GMS) to estimate the clear-sky SW flux. Clear-sky surface fluxes were identified when $\alpha_{\rm vis}$ was small, when the surface measurements were within the 3-h time span of satellite measurements, and when the time variation of the total surface flux was in conformity with that of the insolation at the top of the atmosphere (TOA). Instead of using the total flux and satellite data, we use the direct and diffuse components of the SW flux measured at Kavieng to estimate the clear-sky flux.[1] This approach will avoid the difficulties in specifying the threshold values of $\alpha_{\rm vis}$ for identifying clear satellite pixels and in matching satellite and surface measurements in both space and time.

In cases when clouds do not block the sun, the total flux is the sum of the clear-sky flux and the radiation scattered by clouds, which is greater than that of clear cases. In such cases, the diffuse flux is larger than that which would be measured without the cloud effect. This type of cloud interference can be identified by the large amount of diffuse radiation contributed from clouds. On the other hand, in cases where cloud cover and optical thickness are both large, the diffuse radiation could be small, but the direct radiation is also small. This type of cloud interference can be easily identified by the small amount of direct radiation. Therefore, clear-sky radiation measurements can be identified by simultaneously observing the following conditions:

1) The direct downward SW flux is a maximum for a given solar zenith angle. The maximum should decrease with increasing solar zenith angle.
2) The diffuse downward SW flux is a minimum for a given solar zenith angle.
3) The total surface SW flux varies smoothly with time, in concert with the insolation at TOA.

At the Kavieng station, there are over 20 000 1-min resolution measurements month^{-1} for each of the direct and diffuse flux components. Based on the conditions given above, we identify clear-sky fluxes either for the individual IOP months (method 1) or for the entire IOP (method 2). Results of these two approaches are then compared. The insolation at TOA varies by 0.5%–1.3% ($\approx$7–18 W m^{-2}) in each of the four months. Therefore, the measured fluxes are normalized by multiplying a factor $\overline{S_m}/S_i$ when clear-sky fluxes are estimated using

[1] A separate method was devised by Long (1996) to estimate the clear-sky SW fluxes using the ratio of the diffuse flux to the total flux.

method 1, and by $\overline{S}/S_i$ when clear-sky fluxes are estimated using method 2, where S_i, $\overline{S_m}$, and $\overline{S}$ are the mean TOA insolation of the day i, of the month m, and of the entire IOP, respectively. The following steps are then taken to identify clear-sky surface fluxes:

1) Delete all the data with a large ratio of $F_{\text{dif}}/F_{\text{tot}}$ (e.g., >0.6), which are apparently cloud contaminated, where F_{dif} and F_{tot} are, respectively, the diffuse and total downward SW fluxes.
2) Fit the remaining data points in the $\mu_o - F_{\text{dif}}$ scatterplot with a smooth function (third polynomial) and delete all points with $F_{\text{dif}}(\mu_o) > P_{\text{dif}}(\mu_o) + \delta_{\text{dif}}$, where μ_o is the cosine of the solar zenith angle, P_{dif} is the polynomial fit, and δ_{dif} is a specified threshold value.
3) Fit the remaining data after the above step with a smooth function in the $\mu_o - F_{\text{dir}}$ scatterplot and delete all the points with $F_{\text{dir}}(\mu_o) < P_{\text{dir}}(\mu_o) - \delta_{\text{dir}}$, where F_{dir} is the direct downward SW flux, P_{dir} is the polynomial fit, and δ_{dir} is a specified threshold value.
4) Continue repeating the last two steps.

The regression functions $P_{\text{dir}}(\mu_o)$ and $P_{\text{dif}}(\mu_o)$ are taken to be the mean clear-sky fluxes and the thresholds δ_{dir} and δ_{dif} are taken to be half the range in F_{dir} and F_{dif} variations, respectively, due to variations in the water vapor amount and aerosol loading. After a number of iterations of steps 2–3, the remaining points in the scatterplots are then taken to be clear-sky measurements without cloud interference. Since $P_{\text{dir}}(\mu_o)$ and $P_{\text{dif}}(\mu_o)$ are the mean clear-sky fluxes, it is expected that the clear-sky fluxes scatter evenly around $P_{\text{dir}}(\mu_o)$ and $P_{\text{dif}}(\mu_o)$ with a maximum spread of $\approx\delta_{\text{dir}}$ and δ_{dif}, on either side of these curves. Those cases identified as clear-sky measurements will have the following features in the scatterplots:

1) Points of $F_{\text{dif}}(\mu_o)$ are all less than the smooth curve $P_{\text{dif}}(\mu_o) + \delta_{\text{dif}}$.
2) Points of $F_{\text{dir}}(\mu_o)$ are all greater than the smooth curve $P_{\text{dir}}(\mu_o) - \delta_{\text{dir}}$.
3) For a given μ_o, the clear-sky measurements have a maximum F_{dir} and a minimum F_{dif}.
4) The clear-sky total downward flux, $F_{\text{dir}} + F_{\text{dif}}$, is a smooth function of time (or μ_o).

Values of δ_{dir} and δ_{dif} are judicially specified. In the TOGA COARE region during the IOP, the column-integrated water vapor amount varies by a factor of 2, or approximately between 3.5 and 6.5 g cm^{-2}. The effect of water vapor on the downward SW flux at the surface is shown in the upper panel of Fig. 1 for a solar zenith angle of 60°. It is calculated using a radiation model addressed in the next section. It can be seen in the figure that the surface SW flux is reduced by $\approx$15 W m^{-2} for the column water vapor increasing from 3.5 g cm^{-2} to 6.5 g cm^{-2}. For a smaller solar zenith angle, the variation in the surface flux due to water vapor is between 15 and 30 W m^{-2}. The aerosol optical thickness in the IOP

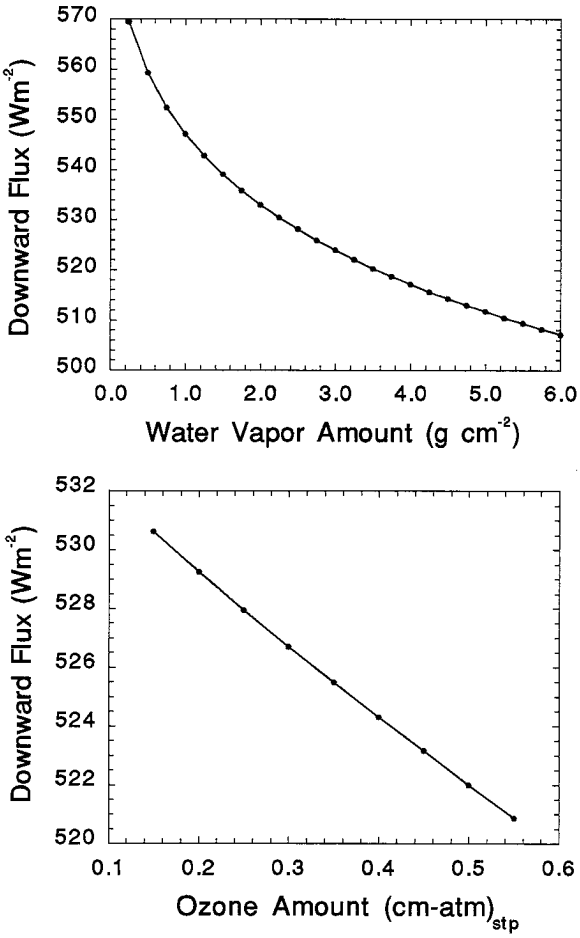

FIG. 1. The downward surface SW flux as a function of the column water vapor amount (upper panel) and ozone amount (lower panel) computed with a solar zenith angle of 60°.

is estimated to be 0.12 nearly evenly divided between the stratosphere and the troposphere (more details are given in the next section). Within a month, the aerosol optical thickness varies only slightly in the stratosphere, and the variation in the total optical thickness is expected to be predominately in the troposphere. Assuming the tropospheric aerosol optical thickness varies by 0.04 (out of a mean of 0.07) in a month, the effect is approximately 40 W m^{-2} on F_{dir} and 25 W m^{-2} on F_{dif} for $\mu_o \to 1$ when the magnitude of clear-sky surface SW flux is $\approx$1000 W m^{-2}. Therefore, we estimate that the variation in F_{dir} due to variations in water vapor and aerosol is $\approx$60 W m^{-2}, and the threshold δ_{dir} is specified at 30 W m^{-2}. The threshold δ_{dif} is set to 10 W m^{-2}, which is roughly half of the variation in F_{dif} due to the variation in aerosol optical thickness.

The results of the clear-sky surface flux estimation using method 1 are shown in Figs. 2–5 and those using method 2 are shown in Fig. 6. The curves in the upper and lower panels are the estimates P_{dir} and P_{dif}, respectively. Points in the figures are the flux measurements

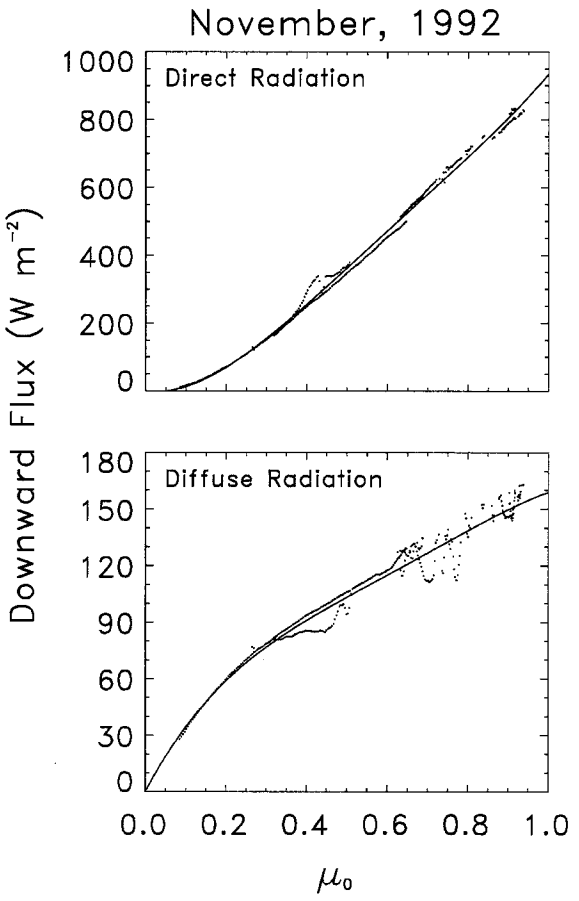

FIG. 2. Estimation of the downward clear-sky SW flux as a function of the cosine of solar zenith angle (μ_o) using method 1 at Kavieng for January 1992. Dots are from surface measurements, and curves are polynomial fits to data points.

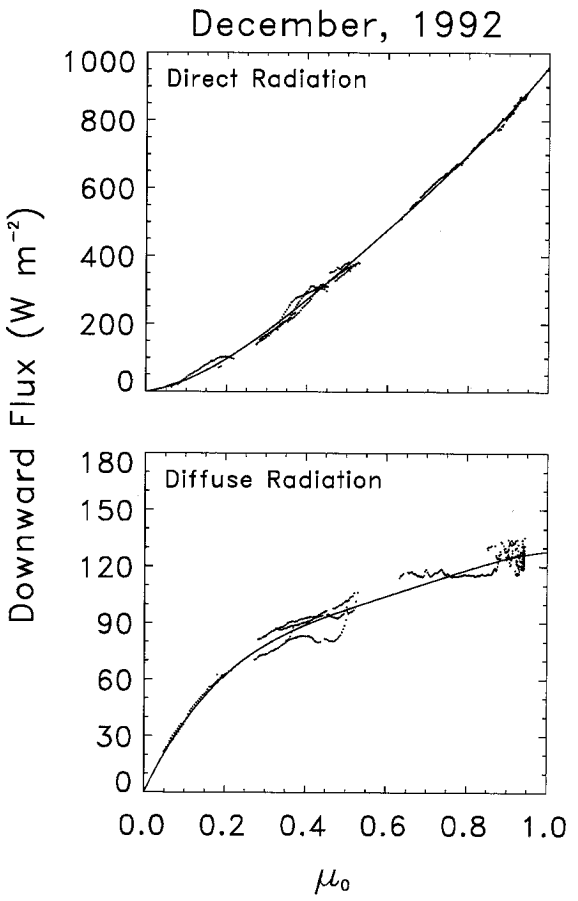

FIG. 3. Same as in Fig. 2 except for December 1992.

normalized either by $\overline{S_m}/S_i$ (Figs. 2–5) or by $\overline{S}/S_i$ (Fig. 6). They all meet the conditions $F_{\text{dir}}(\mu_o) > P_{\text{dir}}(\mu_o) - 30$ W m^{-2} and $F_{\text{dif}}(\mu_o) < P_{\text{dif}}(\mu_o) + 10$ W m^{-2}, and are identified as clear-sky measurements. These results are obtained after a number of iterations of steps 2–3 of the clear-sky identification procedures mentioned above. Figure 7 shows the number of remaining surface measurements after each iteration when method 2 is used. The number of points that meet the above-mentioned conditions converges, and so do the functions $P_{\text{dir}}(\mu_o)$ and $P_{\text{dif}}(\mu_o)$ (not shown in the figure), after the 12th iteration. Out of a total of over 80 000 1-min radiation measurements in the IOP, there are 1354 measurements identified as free of cloud interference, which are the data points shown in Fig. 6.

Clear-sky fluxes individually estimated for each month using method 1 could differ significantly, especially for the diffuse component (Figs. 2–5). For example, the estimated clear-sky diffuse flux for November 1992 and February 1993 is larger than that for December 1992 and January 1993 by 20–30 W m^{-2} for $\mu_o > 0.65$. The cause for this discrepancy is not clear. It could be due to variations in the aerosol loading and water vapor amount, errors in flux measurements, or deficiencies in the clear-sky identification scheme. Generally, a smaller diffuse flux estimation in a month is accompanied by a larger direct flux estimation. Figure 6 shows the clear-sky flux estimations using all the radiation measurements in the IOP (method 2). As expected, there are many more measurements identified as free of cloud interference than the individual months. The curves P_{dir} and P_{dif} vary very smoothly with μ_o.

The surface downward clear-sky flux estimated for February 1993 using method 2 is shown by the solid curve in Fig. 8. It is the sum of the curves in Fig. 6 multiplied by $\overline{S_m}/\overline{S}$, where $\overline{S_m}$ and $\overline{S}$ are the mean TOA insolation in February 1993 and in the IOP, respectively. Also shown in the figure are the TOA insolation (dashed curve) and the 1-min surface radiation measurements (dots) in February 1992. The mean transmission of the atmosphere, which is the ratio of the solid curve to the dashed curve, is 0.75 for $\mu_o \approx 1$ and 0.65 for $\mu_o \approx 0.5$. There are many points substantially above the solid line, indicating a large enhancement of surface flux due to scattering of SW radiation by clouds. In a few cases, the surface radiation is even greater than the TOA in-

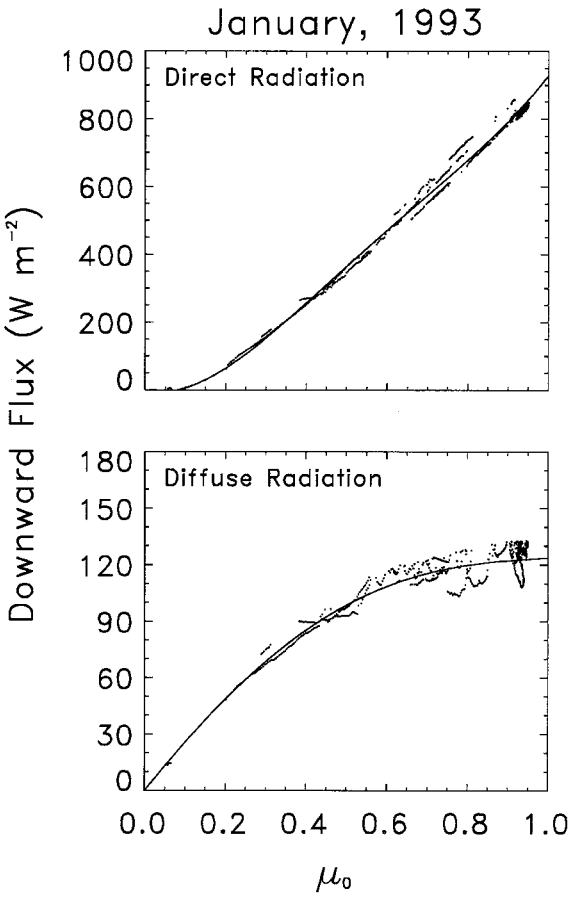

FIG. 4. Same as in Fig. 2 except for January 1993.

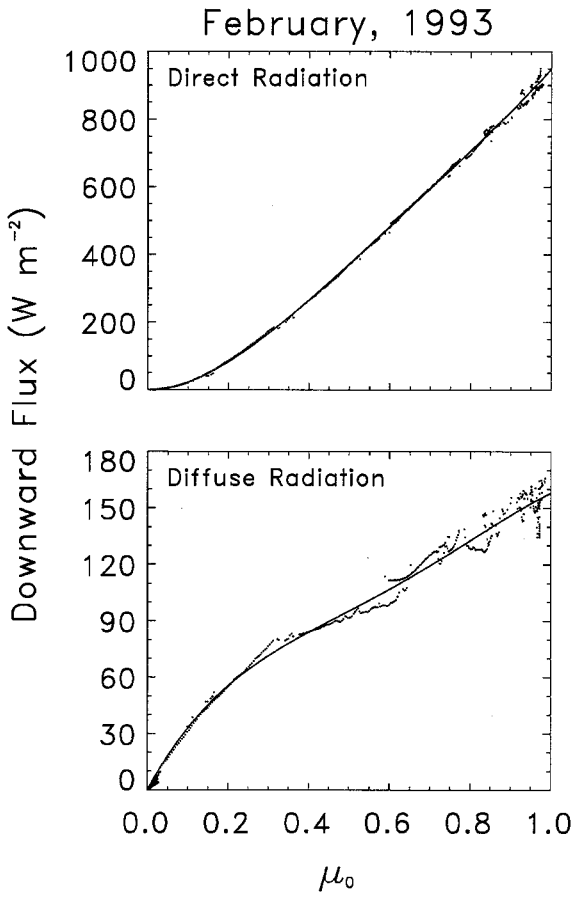

FIG. 5. Same as in Fig. 2 except for February 1993.

solation. The maximum values of the measured downward SW fluxes for a given solar zenith angle have often been used to estimate the clear-sky fluxes (e.g., Cess et al. 1995). From the results shown in the figure, it is clear that the maximum values of the surface SW radiation do not provide adequate information for estimating clear-sky fluxes in strong convective regions. Separate measurements of the direct and diffuse components of the total flux are very useful for estimating clear-sky fluxes.

Figure 9 shows the monthly mean diurnal variations of direct, diffuse, and total clear-sky downward fluxes estimated using method 2. Data points are the clear-sky measurements (corresponding to the data points in Fig. 6), and the curves are the diurnal clear-sky fluxes derived from P_{dir} and P_{dif} (also shown in Fig. 6) and multiplied by $S_m/\overline{S}$. Since only a single pair of P_{dir} and P_{dif} are derived in this case, the curves of the different months differ only by a factor $S_m/\overline{S}$. It can be seen in the figure that there are gaps in time when no clear-sky measurements are identified, indicating a strong cloud interference on the surface radiation.

The estimated monthly mean downward surface SW fluxes are given in Table 2. To investigate the sensitivity of the clear-sky flux estimation to δ_{dir} and δ_{dif}, we reduce these thresholds by half to 15 and 5 W m^{-2}, respectively. The results are presented as method 3. Method 3 is the same as method 2, except for the reduced threshold values. As can be seen in the table, estimations using methods 1 and 2 differ by $\approx$10 W m^{-2} in January 1993. Averaged over the four months, difference in the direct flux estimations is largely offset by that in the diffuse flux estimations, and the estimated total downward clear-sky fluxes differ by only 2 W m^{-2} between method 1 and method 2. When the values of δ_{dir} and δ_{dif} are reduced by half (method 3), only those measurements with very small diffuse flux and very large direct flux are identified as free of cloud interference. As a result, the direct flux is larger, by 2 W m^{-2}, and the diffuse flux is smaller, also by 2 W m^{-2}, when compared to that of method 2. The monthly variation in the total clear-sky flux is $\approx$14 W m^{-2}, which is primarily caused by the monthly variation in the TOA insolation. Averaged over the four months, the total downward surface SW flux remains practically the same for all the three methods. Approximately 85% of the total clear-sky flux is contributed from the direct component.

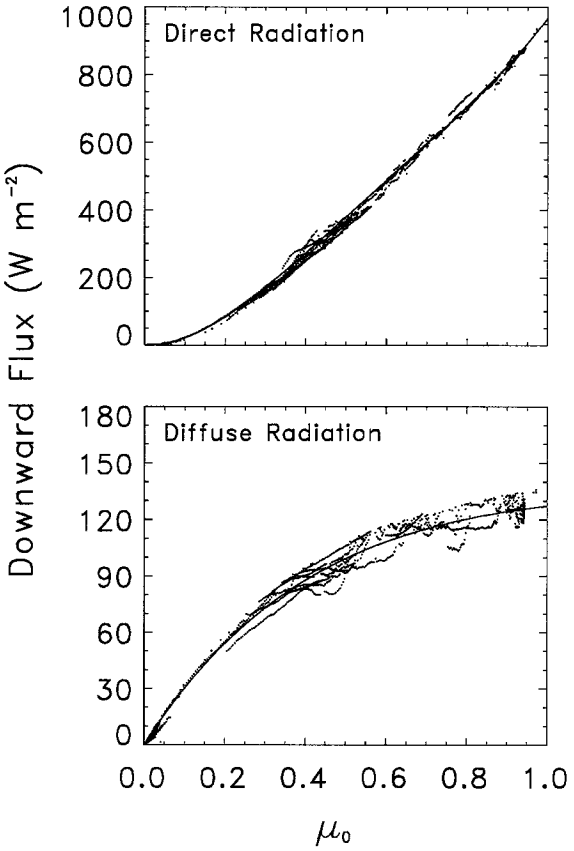

FIG. 6. Estimation of the downward clear-sky SW flux as a function of the cosine of solar zenith angle (μ_o) using method 2 at Kavieng for the four IOP months, November 1992–February 1993. Dots are from surface measurements, and curves are polynomial fits to data points.

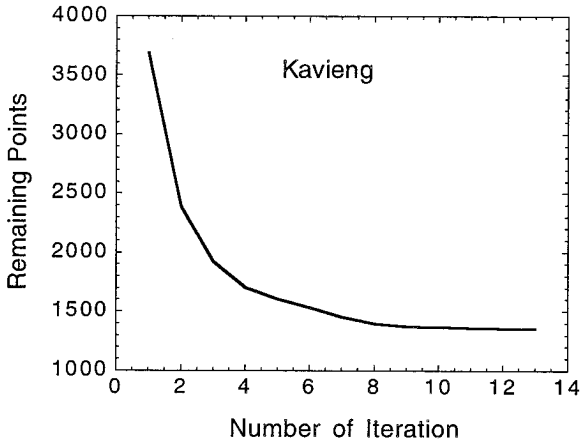

FIG. 7. Number of the remaining surface SW measurements after each screening iteration (steps 2–3 of the clear-sky identification procedures) using method 2.

4. Radiative transfer calculations

The estimated clear-sky downward SW fluxes shown in Table 2 are used to validate radiation model calculations. In computing fluxes, the solar spectrum is divided into shortwave (wavelength < 0.7 μm) and near-infrared (wavelength > 0.7 μm) regions. Absorption due to ozone and scattering due to molecules (Rayleigh scattering) are included in the shortwave region, and absorption due to water vapor, O_2 and CO_2 are included in the near IR (Chou 1990; Chou and Lee 1996). Scattering and absorption due to aerosols are included in both the shortwave and near IR regions. The ozone absorption coefficient varies smoothly with wavelength and is nearly independent of pressure and temperature. The shortwave spectrum is grouped into eight bands, and an effective ozone absorption coefficient and an effective Rayleigh scattering coefficient are given for each of the eight bands. The near IR is divided into three water vapor absorption bands. The *k*-distribution method with a simple pressure-scaling is used to compute the absorption due to water vapor. In each of the three water vapor bands, ten *k*-distribution functions (or 10 values of the absorption coefficient, *k*) are used. The delta-Eddington approximation (Joseph et al. 1976) is used to compute the multiple scattering due to aerosols and atmospheric gases. The radiation model is fast and accurate. Compared to high spectral resolution calculations of ozone absorption and line-by-line calculations of water vapor absorption, errors in the surface SW flux are $<1\%$.

In comparing the surface SW fluxes calculated from models with that estimated from surface measurements, it is important to understand the sensitivity of SW radiation to the concentrations and extinction coefficients of water vapor, ozone, and aerosols. Figure 1 shows the effects of water vapor (upper panel) and ozone (lower panel) amounts on the surface downward flux for a solar zenith angle of 60°. The effect of Rayleigh scattering and O_2 and CO_2 absorption are included in the calculations, but not the effects of clouds and aerosols. The temperature profile is taken from the typical tropical atmosphere given in McClatchey et al. (1972). It is found that temperature has a very little effect on flux calculations. When varying the column-integrated water vapor amount (upper panel) or ozone amount (lower panel), the shapes of the water vapor and ozone vertical profiles are fixed at that of the tropical atmosphere. The ranges of water vapor and ozone amounts shown in the figure are typical of the earth's atmosphere. It can be seen in the figure that the surface radiation reduces by $\approx$1.5 W m^{-2} for a 10% increase in the column water vapor amount, which is $\approx$0.3% of the clear-sky surface SW radiation with a solar zenith angle of 60°. For the ozone absorption, the effect is even smaller. The surface SW flux changes by only 8 W m^{-2} (or $\approx$2%) for the entire span of the ozone amount found in the earth's atmosphere, from 0.18 to 0.50 (cm-atm)$_{stp}$. The reason for this insensitivity is the strong absorption in the ultraviolet region with wavelength less than 0.3 μm. Due to the strong absorption, surface SW radiation in this

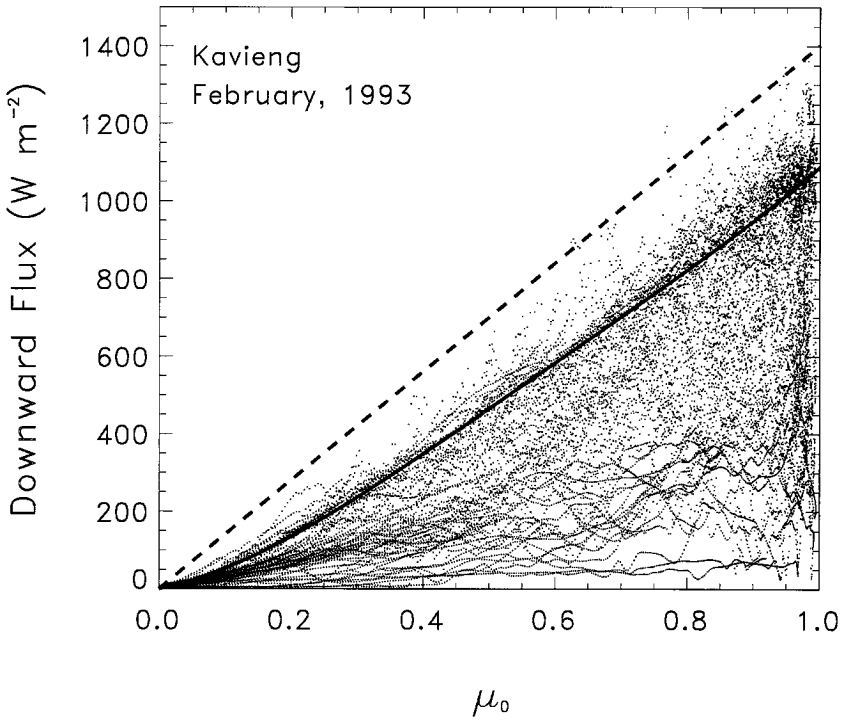

FIG. 8. The total downward SW flux measured at Kavieng for February 1992. Dots are 1-min resolution measurements, the dashed curve is the insolation at the top of the atmosphere, and the solid curve is the estimated clear-sky flux using method 2.

spectral region is small, and a perturbation in the ozone amount has a little effect on the surface SW heating. However, the ozone amount has a significant effect on the vertical distribution of SW heating in the middle atmosphere. Based on these results and assuming an uncertainty of $<20\%$ in water vapor sounding, the error in surface SW radiation calculations induced by the uncertainties in water vapor and ozone amounts is estimated to be <3 W m^{-2}, or $<1\%$.

Daily variations of the vertically integrated water vapor amount and the model-calculated downward surface SW flux are shown in Fig. 10 for the Kavieng station during the IOP. The TOA insolation varies by ≈ 26 W m^{-2} in the four TOGA COARE months, and the result shown in the figure is the flux normalized by $\overline{S}/S_i$. The first of November 1992 is assigned to day 1. Fluxes are calculated at 15-min intervals and then averaged over a day. Aerosols are included in the calculations, which is to be discussed latter. It can be seen in the figure that the water vapor amount varies by a factor of ≈ 2, from 3.5 to 6.5 g cm^{-2}. As expected, the daily variation of the surface flux follows exactly that of the water vapor amount, but in the opposite direction. The daily averaged downward flux varies by ≈ 8 W m^{-2}, approximately from 306 to 314 W m^{-2}.

Since scattering due to water vapor and ozone is negligible, the optical thickness is a product of the absorption coefficient and the absorber amount. Therefore, a given percentage error in the absorber amount and in the absorption coefficient will cause the same error in flux calculations. The conclusion on the sensitivity to water vapor and ozone amounts can also be applied to the absorption coefficient. For example, a 20% increase in the water vapor absorption coefficient uniformly across the near IR region will cause a reduction of ≈ 3 W m^{-2} in the surface SW radiation. The surface SW radiation is not sensitive to uncertainties in the ozone absorption coefficient.

Depending upon the optical thickness, aerosols could have a significant effect on the surface SW radiation. In remote oceanic regions, aerosols are predominantly sulfuric formed from the emission of dimethylsulfide (DMS) by phytoplanktons. The emission of DMS is a function of water temperature, sunlight, and nutrient, while the particle size of aerosols is affected by atmospheric relative humidity. Due to high relative humidity in the Pacific warm pool, biogenic sulfate aerosols may have a significant impact on surface radiation. The TOGA COARE IOP is about 1.5 yr after the Pinatubo volcanic eruptions. Stratospheric aerosol extinction profiles during this period were derived for 4 spectral bands, ranging from 0.385 to 1.02 μm, from the SAGE II (Stratospheric Aerosol and Gas Experiment II) measurements. The vertically integrated optical thickness of the remnant Pinatubo aerosols in the Tropics is mostly between 0.04 and 0.06. Information on the tropospheric aerosol in the TOGA COARE during the IOP is lacking.

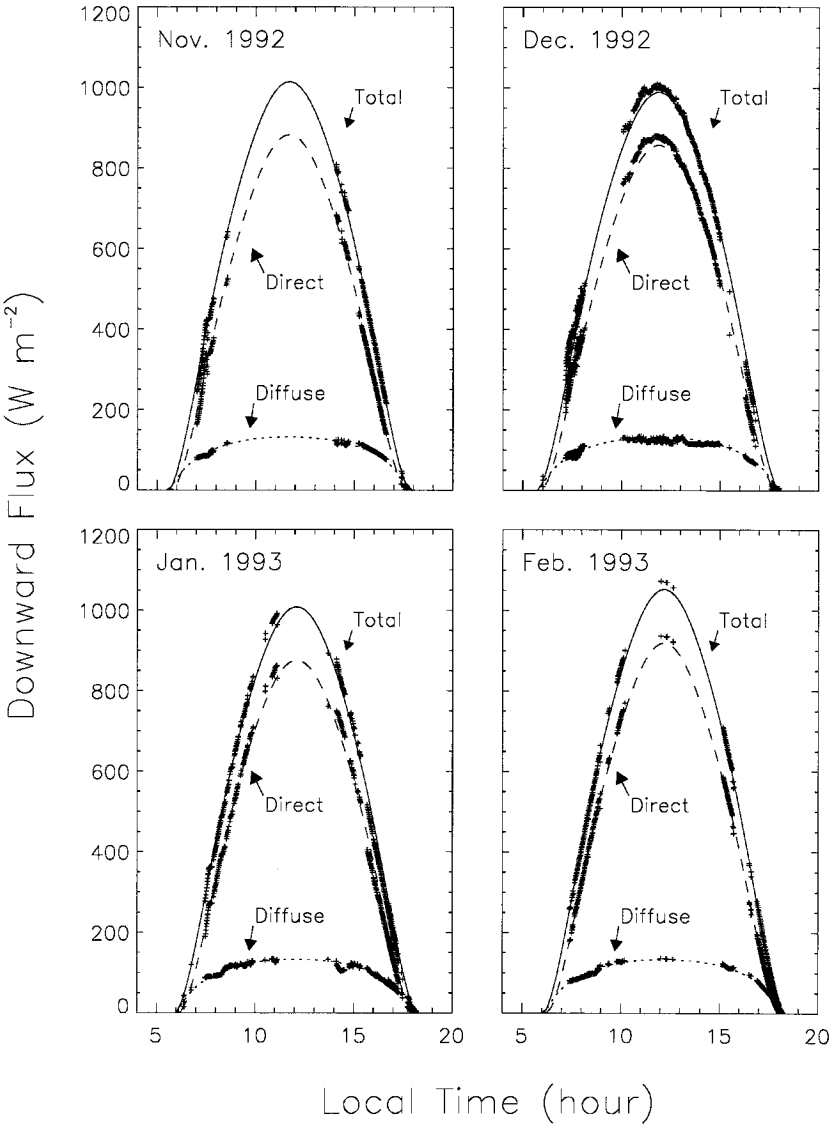

FIG. 9. Monthly mean diurnal variations of the clear-sky downward SW fluxes at Kavieng estimated using method 2. Dots are 1-min clear-sky measurements, and the curves are regressions corresponding to the curves in Fig. 6.

Due to inadequate information on aerosol optical properties, the aerosol optical thickness and asymmetry factor are determined by matching the direct and diffuse surface fluxes from model calculations with that estimated from the surface measurements. In the model calculations, temperature and humidity are interpolated from the radiosonde measurements, which has a 6-h temporal resolution. The ozone vertical profile is taken from the typical tropical atmosphere of McClatchey et al. (1972). Clouds are not included. Stratospheric volcanic aerosols and tropospheric aerosols in the marine boundary layer are mostly sulfuric aerosols, which have a weak absorption in the solar spectrum. In this study, we assume that the effect of aerosols on the SW radiation is primarily scattering, and the aerosol single-scattering albedo is set to 0.995. The sulfuric aerosols are submicrometer particles, and the asymmetry factor should be significantly smaller than that of cloud water droplets, which have a mean size of ≈ 10 μm and an asymmetry factor of ≈ 0.84. It is found from model calculations that the clear-sky direct and diffuse fluxes estimated from radiation measurements can be well reproduced with $\tau_a = 0.12$ and $g = 0.5$, where τ_a is the aerosol optical thickness, and g is the asymmetry factor. From SAGE II measurements, the optical thickness of stratospheric aerosols in the Tropics is ≈ 0.05 and varies only slightly with wavelengths from 0.385 to 1.02 μm. Therefore, the aerosol optical thickness, single-scattering albedo, and asymmetry factor are assumed to be independent of wavelength in flux calculations. Of the

TABLE 2. Monthly mean clear-sky downward SW fluxes at Kavieng estimated from surface measurements and calculated from radiation models. Estimations of clear-sky fluxes are based on measurements in individual months for method 1 and on all measurements in the four IOP months for method 2. Method 3 is the same as method 2, except values of the thredholds, δ_{dir} and δ_{dif}, are reduced by half. Units are W m^{-2}.

	November 1992	December 1992	January 1993	February 1993	Mean
			Direct flux		
Estimation					
Method 1	251	253	247	267	254
Method 2	258	252	257	267	258
Method 3	260	254	259	269	260
Model calculation	262	254	258	268	260
			Diffuse flux		
Estimation					
Method 1	56	50	49	55	52
Method 2	50	50	50	50	50
Method 3	47	47	48	48	48
Model calculation	50	50	50	50	50
			Total flux		
Estimation					
Method 1	308	303	296	322	306
Method 2	308	302	307	317	308
Method 3	308	301	307	317	308
Model calculation	312	304	308	318	310

total of 0.12, an optical thickness of 0.05 is assumed to be in the stratosphere and 0.07 in the troposphere. Figure 11 shows the diurnal distribution of the difference between the model-calculated downward fluxes with and without aerosols at Kavieng for February 1993. Fluxes are computed at 15-min intervals and then averaged over the entire month to get the mean diurnal variation. It can be seen in the figure that the effect of aerosols on the downward surface flux reaches 32 W m^{-2}. Averaged over the month, the effect is ≈13 W m^{-2}, or ≈4% of the clear-sky surface radiation. The albedo at TOA increases by 3%, from 8% without aerosols to 11% with aerosols. The SW heating of the atmosphere is ≈90 W m^{-2} both with and without aerosols, or ≈20% of the insolation at TOA. Table 2 compares the estimated and model-calculated downward fluxes at the surface. The clear-sky flux calculated from the model is within a few watts per squared meter of that estimated from TOGA COARE measurements.

5. Cloud radiative forcing

The effect of clouds on radiative flux, or cloud radiative forcing (CRF), is defined as the difference between the all-sky flux and the clear-sky flux. The downward all-sky flux was measured at all the radiation stations. Due to some missing data, derivation of the daily flux for each day is not possible. Therefore, we first composite the diurnal variation of the surface flux from measurements for each of the four TOGA COARE

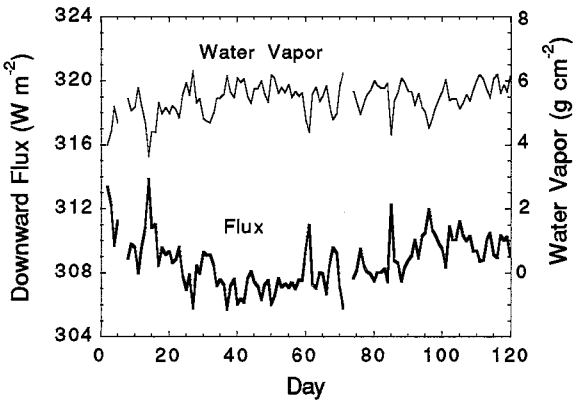

FIG. 10. Daily-mean column-integrated water vapor amount and clear-sky downward SW flux at Kavieng for the four IOP months. The clear-sky downward flux is from model calculations. The first of November 1992 is assigned to day 1.

months, and then compute the monthly mean all-sky surface flux. On the other hand, identification of clear-sky flux from the surface measurements is difficult for the stations other than Kavieng because the direct and diffuse components of the SW flux were not separately measured. Therefore, we use the aerosol optical properties inferred for the Kavieng station and the radiosonde measurements of temperature and humidity at individual stations to calculate the clear-sky fluxes. At the IMET buoy and Manus station, there were either no radiosonding or no reliable radiosonding available. We use the soundings from the nearest sites to compute SW fluxes at these two stations. The error induced by this assumption is small as the sensitivity of the surface SW radiation to variations in temperature and humidity is weak. The clear-sky downward SW fluxes are computed at 15-min intervals. Temperature and humidity profiles

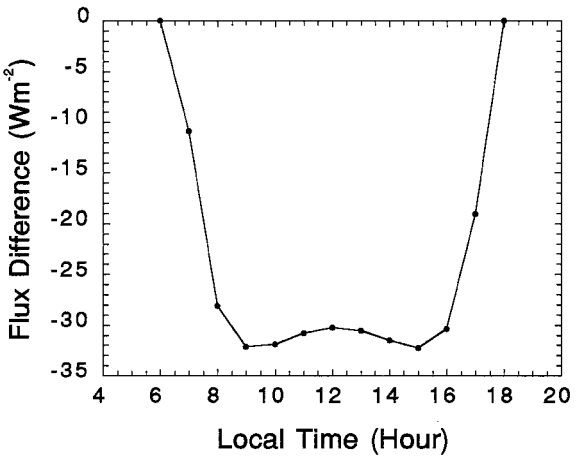

FIG. 11. Diurnal distribution of the aerosol effect on the net downward clear-sky surface SW flux at Kavieng for February 1993. The aerosol optical thickness, single-scattering albedo, and asymmetry factor are set at 0.12, 0.995, and 0.5, respectively.

TABLE 3. Clear-sky and all-sky *net* solar fluxes and cloud radiative forcing (CRF) at the surface averaged over the four TOGA COARE IOP months. The clear-sky fluxes are model calculations, and the all-sky fluxes are from surface measurements. Units are W m^{-2}.

	Clear-sky	All-sky	CRF
IMET	300	196	104
Kapingamarangi	300	198	102
Kavieng	297	190	107
Kexue	298	210	88
Manus	297	218	79
Nauru	300	188	112
Shiyan	298	199	99
Average	299	200	99

are interpolated from the radiosonde measurements that have a temporal resolution of 6 h.

The albedo at the ocean surface depends on the incident angle of the radiation. In computing clear-sky fluxes, the surface albedo is precomputed from Fresnel equation for both direct and diffuse radiation. The albedo of direct radiation is in the range 0.02–0.04 for the solar zenith angle $<53°$ but increases rapidly for larger angles. The albedo of diffuse radiation is computed by integrating the directional albedo over the sphere assuming isotropic radiation, which is found to be ≈ 0.06. These surface albedos are used in the radiation model calculations of clear-sky fluxes. For all-sky fluxes, the surface albedo depends on the solar zenith angle and cloudiness (or equivalently the ratio of diffuse to direct fluxes). Using the direct and diffuse components of surface fluxes measured at Kavieng, the surface albedo for all-sky fluxes is calculated for the four TOGA COARE months. It is found to be ≈ 0.05 for all of the four months. Therefore, the all-sky net downward flux at the surface is derived by multiplying the measured downward flux by 0.95.

The clear-sky and all-sky net SW fluxes and CRF at the surface averaged over the four TOGA COARE IOP months are given in Table 3. As can be expected, variation in the clear-sky surface flux among the seven radiation stations is small (3 W m^{-2}), but variation in the all-sky surface flux is large (30 W m^{-2}). As a result of the large all-sky flux variation, the range of SW CRF is also large, from 79 to 112 W m^{-2}. Averaged over all these stations, the SW CRF is 99 W m^{-2}. Table 4 compares the net downward SW flux and CRF of this study with that of Waliser et al. (1996) and Long (1996). Our estimate of CRF at IMET (104 W m^{-2}) is close to the estimates by Waliser et al. (103 and 107 W m^{-2} using two different methods), and our estimate of the SW CRF of 100 W m^{-2} in the TOGA COARE IFA is close to 92 W m^{-2} as estimated by Long (1996). Our estimate of clear-sky flux is close to that of Waliser et al. (1996) but is larger than that of Long (1996) by 13 W m^{-2}. It is noted that all-sky fluxes are directly derived from radiation measurements. The discrepancies shown in the table, ≈ 5 W m^{-2}, are believed to be due to the different methods that monthly mean fluxes are computed, the use of different surface albedos, and the different methods that fluxes are averaged in the IFA.

TABLE 4. Comparison of the estimated *net* downward SW fluxes and cloud radiative forcing (CRF) at the surface with that of the other studies. Units are W m^{-2}.

	Clear-sky	All-sky	CRF
	IMET		
This study	300	196	104
Waliser	294–298	191	103–107
	Intensive flux array		
This study	299	199	100
Long	286	194	92

6. Conclusions

The TOGA COARE radiation measurements during the Intensive Observation Period (IOP) provide very useful data for studying the surface radiation budgets in the Pacific warm pool and for validating radiation model calculations. Cloudiness in the warm pool is large. Even in relatively calm periods, low clouds are ubiquitous. Measurements of total surface SW radiation alone do not provide adequate information for identifying clear-sky SW radiation. The Atmospheric Radiation Measurements site at Kavieng measured both direct and diffuse downward surface SW fluxes at high temporal resolution (1 min). These data are used to identify clear-sky SW radiation by simultaneously imposing the conditions that for a given solar zenith angle the direct downward flux is a maximum and the diffuse downward flux is a minimum, and that the total SW radiation varies smoothly with time. Of more than 20 000 1-min measurements $month^{-1}$, only a few hundreds are identified as clear-sky measurements without cloud interference. Averaged over the four TOGA COARE months, the clear-sky downward SW flux is 308 W m^{-2}, with a range of 301–317 W m^{-2}.

The estimated clear-sky SW fluxes together with the temperature and humidity radiosonding at Kavieng are used to validate radiation model calculations. Aerosols have a significant effect on the surface SW radiation. The model-calculated direct and diffuse SW fluxes are made to agree with that of measurements by setting the aerosol optical thickness to 0.12, asymmetry factor to 0.5, and the single-scattering albedo to 0.995. Without introducing aerosols, the model-calculated downward flux is significantly larger than that estimated from measurements. Averaged over a day, the difference is 13 W m^{-2}. Based on the SAGE II measurements, the stratospheric aerosol optical thickness is inferred to be ≈ 0.05 in the Tropics, which is the residue of the June 1991 Pinatubo volcanic eruptions. The tropospheric aerosol optical thickness is then ≈ 0.07, which is a reasonable number in remote oceanic regions. Therefore, we can conclude that clear-sky surface SW fluxes can be reliably computed using a radiation model.

The cloud effect on the surface SW radiation is estimated by taking the difference between the measured all-sky radiation and the model-calculated clear-sky radiation at the surface for all the TOGA COARE radiation stations. The aerosol optical properties inferred from the radiation measurement at Kavieng is applied to all other stations in computing clear-sky fluxes. Variation in the net clear-sky surface fluxes among the seven radiation stations is small (3 W m^{-2}) with a mean of 299 W m^{-2} over the four TOGA COARE months. The range of the cloud radiative forcing among stations is large, from 79 to 112 W m^{-2}, which is a result of a large variation in all-sky fluxes. Averaged all these stations, the cloud radiative forcing is 99 W m^{-2}, which is in agreement with the results of some recent studies.

Acknowledgments. This study was supported by the Radiation Research Program and EOS Interdisciplinary Research Program, NASA/Office of Mission to Planet Earth. The assistance of Charles Long and Charles Parloski of The Pennsylvania State University in accessing ARM PROBE data is greatly appreciated.

REFERENCES

Arking, A., M.-D. Chou, and W. L. Ridgway, 1996: On estimating the effects of clouds on atmospheric absorption based on flux observations above and below cloud level. *Geophys. Res. Lett.,* **23,** 829–832.

Cess, R. D., and Coauthors, 1995: Absorption of solar radiation by clouds: Observations versus models. *Science,* **267,** 496–499.

Charlock, T. P., and T. L. Alberta, 1996: The CERES/ARM/GEWEX Experiment (CAGEX) for the retrieval of radiative fluxes with satellite data. *Bull. Amer. Meteor. Soc.,* **77,** 2673–2683.

Chou, M.-D., 1990: Parameterization for the absorption of solar radiation by O_2 and CO_2 with application to climate studies. *J. Climate,* **3,** 209–217.

——, 1994: Radiation budgets in the western tropical Pacific. *J. Climate,* **7,** 1958–1971.

——, and K.-T. Lee, 1996: Parameterizations for the absorption of solar radiation by water vapor and ozone. *J. Atmos. Sci.,* **53,** 1203–1208.

——, A. Arking, J. Otterman, and W. L. Ridgway, 1995: The effect of clouds on the atmospheric solar heating. *Geophys. Res. Lett.,* **22,** 1885–1888.

Hayasaka, T., N. Kikuchi, and M. Tanake, 1995: Absorption of solar radiation by stratocumulus clouds: Aircraft measurements and theoretical calculations. *J. Appl. Meteor.,* **34,** 1047–1055.

Imre, D. G., E. H. Abramson, and P. H. Daum, 1996: Quantifying cloud-induced shortwave absorption: An examination of uncertainties and of recent arguments for large excess absorption. *J. Appl. Meteor.,* **35,** 1991–2010.

Joseph, J. H., W. J. Wiscombe, and J. A. Weinman, 1976: The delta-Eddington approximation for radiative flux transfer. *J. Atmos. Sci.,* **33,** 2452–2459.

Li, Z., and L. Moreau, 1996: Alteration of atmospheric solar absorption by clouds: Simulation and observation. *J. Appl. Meteor.,* **35,** 653–670.

Long, C. N., 1996: Surface radiative energy budget and cloud forcing: Results from TOGA COARE and techniques for identifying and calculating clear sky irradiance. Ph.D. dissertation, The Pennsylvania State University, 139 pp. [Available from Dept. of Meteorology, The Pennsylvania State University, 503 Walker Building, University Park, PA 16802.]

McClatchey, R. A., R. W. Fenn, J. E. A. Selby, F. E. Volz, and J. S. Garing, 1972: Optical properties of the atmosphere. 3d ed. AFCRL-72-0497, 108 pp. [NTIS N7318412.]

Parsons, D., and Coauthors, 1994: The integrated sounding system: Description and preliminary observations from TOGA COARE. *Bull. Amer. Meteor. Soc.,* **75,** 553–567.

Pilewskie, P., and F. P. J. Valero, 1995: Direct observations of excess solar absorption by clouds. *Science,* **267,** 1626–1629.

Ramanathan, V., B. Subasilar, G. J. Zhang, W. Conant, R. D. Cess, J. T. Kiehl, H. Grassl, and L. Shi, 1995: Warm pool heat budget and shortwave cloud forcing: A missing physics? *Science,* **267,** 499–503.

Shi, L., 1994: Cloud radiative forcing on surface shortwave fluxes: A case study based on cloud lidar and radar exploratory test. *J. Geophy. Res.,* **99,** 25 909–25 919.

Waliser, D. E., W. D. Collins, and S. P. Anderson, 1996: An estimate of the surface shortwave cloud forcing over the western Pacific during TOGA COARE. *Geophys. Res. Lett.,* **23,** 519–522.